Stimuli-responsive Janus mesoporous nanosheets towards robust interfacial emulsification and catalysis

Jiangyan Yang,[a#] Jialin Wang,[a#] Yijiang Liu,*[a,b] Huaming Li,[a] Zhiqun Lin*[b]

[a]College of Chemistry, Key Laboratory of Environmentally Friendly Chemistry and Application of Ministry of Education, Xiangtan University, Xiangtan 411105, Hunan Province, China

[b]School of Materials Science and Engineering, Georgia Institute of Technology, Atlanta, GA 30332, USA

Table of Contents

1. Experimental Section

Materials. ZIF-67 was synthesized according to the literature.[1] Cetyltrimethylammonium bromide (CTAB, 99%), tetraethyl orthosilicate (TEOS, 98%), sodium hydroxide (NaOH, 97%), hydrochloric acid (HCl, 9wt%), 2-bromoisobutyryl bromide (BIBB, 98%), copper bromide (CuBr, 99.5%), 4-vinylpyridine (4VP, 95%, pass through neutral Al_2O_3 column prior to polymerization), chloroauric acid ($HAuCl_4$, 98%), sodium borohydride ($NaBH_4$, 98%), 4-nitrophenol (4-NP, 99%), and 4-nitroanisole (98%) were purchased from Sinopharm Chemical Reagent. 3-aminopropyltrimethoxysilane (APTMS, 97%), octadecyltrimethoxysilane (ODTMS, 95%), triethylamine (99.5%), N,N,N',N,'N''-pentamethyldiet hylenetriamine (PMEDTA, 98%) were bought from Alfa Aesar. All these reagents are analytical grade and used without purification unless otherwise noted.

Synthesis of ZIF-67@mSiO$_2$ core@shell NPs. 200 mg of ZIF-67 and 250 mg of CTAB were added into 80 mL of ethanol under ultrasonication. Then, the pH value of the solution was adjusted to pH = 11 via adding 400 μL of NaOH aqueous solution (20 wt%). Afterwards, 450 μL of 30% (v/v) TEOS ethanol solution was added in three portions. The reaction mixture was stirred at room temperature for 18 h. The product was centrifuged and washed with ethanol and water for several times, and dried in an oven at 60 ^{o}C for 12 h to yield ZIF-67@mSiO$_2$ core@shell NPs. In addition, pristine mSiO$_2$ nanosheets could be obtained by etching ZIF-67 under ultrasonication.

Synthesis of OH-mSiO$_2$-NH$_2$ and C$_{18}$-mSiO$_2$-NH$_2$. 200 mg of ZIF-67@mSiO$_2$ and 200 μL of APTMS were dispersed in 40 mL of toluene under ultrasonication. The mixture was heated to 100 ^{o}C and refluxed for 12 h. The crude product was collected by centrifugation, washed with toluene for several times to remove unreacted APTMS, and dried for 12 h in an oven at 70 ^{o}C. The removal of CTAB by Soxhlet extraction in acetone yielded ZIF-67@mSiO$_2$-NH$_2$. After etching ZIF-67 with hydrochloric acid (9 wt%) under ultrasonication, mesoporous Janus nanosheets of HO-mSiO$_2$-NH$_2$ were derived.

The growth of hydrophobic ODTMS onto HO-mSiO$_2$-NH$_2$ was conducted as follows. 100 mg of HO-mSiO$_2$-NH$_2$ and 100 μL of ODTMS were dispersed in 20 mL of toluene. The mixture was then heated to 100 °C and refluxed for 12 h. After cooling down to room temperature, the mixture was centrifuged and washed with toluene for several times to remove the unreacted ODTMS. Amphiphilic mesoporous nanosheets with one side functionalized with hydrophilic amine groups (-NH_2) and the other side grown with hydrophobic ODTMS (referred to as C_{18}) were achieved after drying (denoted C_{18}-mSiO_2-NH_2).

Synthesis of Janus mesoporous nanosheets of HO-mSiO_2-Br. 200 mg of ZIF-67@mSiO_2-NH_2 was dispersed in 20 mL of dichloromethane containing 2% (v/v) triethylamine, and 500 μL BIBB was added after degassed with N_2 in an ice bath. The mixture was stirred for 0.5 h in the ice bath and then reacted at room temperature for 12 h. The resulting product was centrifuged and washed with dichloromethane for several times, yielding Janus mesoporous nanosheets of HO-mSiO_2-Br after removing ZIF-67.

Synthesis of amphiphilic Janus mesoporous nanosheets of C_{18}-mSiO_2-P4VP. Poly(4-vinylpyridine) (P4VP) was grafted from -Br side of HO-mSiO_2-Br through atom transfer radical polymerization (ATRP). The typical procedure was as follows. HO-mSiO_2-Br (150 mg), PMEDTA (50 μL), 4VP (0.4 g), and methanol (10 mL) were mixed in an argon-bubbled ampoule. After degassing by freeze-evacuate-thaw for two times, CuBr (25 mg) was added under argon flow. The ampoule was sealed under vacuum after the third freeze-evacuate-thaw. The polymerization was proceeded at 60 °C for 12 h. The reaction was quenched immediately by liquid nitrogen. The product was washed with methanol several times and dried in an oven at 60 °C for 12 h to yield HO-mSiO_2-P4VP Janus mesoporous nanosheets. Subsequently, the hydroxyl groups (-OH) of HO-mSiO_2-P4VP were converted into hydrophobic octadecyl (C_{18}) using the similar procedure as in the synthesis of C_{18}-mSiO_2-NH_2 described above, yielding amphiphilic Janus mesoporous nanosheets with one side tethered with pH-responsive P4VP and the opposite side anchored with hydrophobic C_{18} (denoted C_{18}-mSiO_2-P4VP).

Crafting of C_{18}-mSiO_2-P4VP@Au and C_{18}-mSiO_2-NH_2@Au. 10 mg of C_{18}-mSiO_2-P4VP was dispersed in 20 mL of ethanol under ultrasonication, and 150 μL of 0.1 mol/L $HAuCl_4$ was then added. The mixture was stirred at room temperature for 12 h. The excess $HAuCl_4$ was removed by centrifugation, and the reactants were re-dispersed in 20 mL of ethanol. Afterwards, freshly prepared $NaBH_4$ (2 mL, 0.1 mol/L) was quickly added and the mixture was further stirred for 2 h. The reactants were centrifuged and washed several times with ethanol. Janus mesoporous nanosheets of C_{18}-mSiO_2-P4VP@Au with Au NPs selectively grown on the P4VP regime were yielded. Similarly, by selectively coordinating Au precursors ($HAuCl_4$) with -NH_2 groups on C_{18}-mSiO_2-NH_2, Janus mesoporous nanosheets of C_{18}-mSiO_2-NH_2@Au were obtained. The synthetic route to control sample of C_{18}-SiO_2-NH_2@Au (SiO_2 without pores) was similar to C_{18}-mSiO_2-NH_2@Au except the absence of CTAB.

Reduction of 4-nitrophenol aqueous solution by employing C_{18}-mSiO_2-P4VP@Au and C_{18}-mSiO_2-NH_2@Au as catalysts. First, 0.1 mmol/L of 4-nitrophenol (4-NP) solution and 0.02 mol/L of $NaBH_4$ solution were prepared in deionized water at pH = 6, respectively. 1 mg of C_{18}-mSiO_2-P4VP@Au (or C_{18}-mSiO_2-NH_2@Au) was then added to the 4-NP aqueous solution (4.5 mL, 0.1 mmol/L) and dispersed under ultrasonication. Afterwards, $NaBH_4$ (0.5 mL, 0.02 mol/L, pH = 6) was quickly added. Aliquots of the reaction mixture were taken out at a certain intervals and analyzed by UV-vis to examine the absorbance of 4-NP. The conversion of 4-NP was calculated according to the absorbance of 4-NP. Similarly, at pH = 12, UV-vis spectra of 4-NP were recorded, and the conversion was calculated. The recycling study on C_{18}-mSiO_2-P4VP@Au (or C_{18}-mSiO_2-NH_2@Au) was carried out after centrifugation and washing with ethanol. Under the identical condition, catalytic reduction of 4-NP using recycled C_{18}-mSiO_2-P4VP@Au (or C_{18}-mSiO_2-NH_2@Au) was performed.

Emulsification of C_{18}-mSiO_2-P4VP@Au and C_{18}-mSiO_2-NH_2@Au. 10 mg of C_{18}-mSiO_2-P4VP@Au was added to the oil/water mixture (1/4 by volume, pH = 6). A Pickering emulsion was formed using an XHF-D high-speed disperser at a stirring rate of 12000 rpm for 1 min. The emulsion droplets were examined using an optical microscope. The de-emulsification of the Pickering emulsion was triggered by adding NaOH (20 wt%) aqueous solution. Similarly, the emulsification and de-emulsification of C_{18}-mSiO_2-NH_2@Au was also conducted in the same manner.

Reduction of 4-nitroanisole at emulsion interface by capitalizing on C_{18}-mSiO_2-P4VP@Au and C_{18}-mSiO_2-NH_2@Au as catalysts. 10 mg of C_{18}-mSiO_2-P4VP@Au was dispersed in the mixture of 4-nitroanisole (0.1 mmol/L, 1 mL) and oil phase (i.e., toluene or octane) under ultrasonication. Then, freshly prepared $NaBH_4$ aqueous solution (0.01 mol/L, 4 mL, pH = 6) was added. The resulting mixture was vigorously stirred to form an oil-in-water emulsion. The reduction of 4-nitroanisole at the Pickering emulsion interface was performed at room temperature. Samples at a certain intervals were withdrawn and centrifuged, thereby breaking emulsion droplets and leading to the formation of two separated layers (i.e., upper oil phase and lower water phase). The upper oil phase was then collected and analyzed by UV-vis to examine the absorbance of 4-nitroanisole. The conversion was calculated according to the absorbance of 4-nitroanisole. C_{18}-mSiO_2-P4VP@Au was reproduced and reused for several times after centrifugation and washing with ethanol. The reduction of 4-nitroanisole using C_{18}-mSiO_2-NH_2@Au as the catalyst was also carried out under identical condition.

2. Characterization

The morphology of as-prepared samples was visualized by scanning electron microscopy (SEM, Hitachi S-4800 at 10KV) equipped with an energy dispersive X-ray (EDX) analyzer and transmission electron microscopy (TEM, JEOL1011 at 100 kV). High-resolution transmission electron microscope (HRTEM) and elemental mapping analysis were performed using JEOL JEM-2100. Atomic force microscopy (AFM) imaging was conducted with Digital Instrument Multimode Nanoscope IIIA operating in a tapping mode. Si MAS spectra were measured by JEOL JNM-ECZ600R spectrometer. Fourier transform infrared (FTIR) spectra of as-prepared samples were measured on a Perkin-Elmer Spectrum One FTIR spectrometer in the range from 4000 cm^{-1} to 400 cm^{-1}. X-ray diffraction (XRD) was conducted on Max-2500PC X-ray diffractometer from Japan Rigaku Company. Au content was measured by using inductively coupled plasma optical emission spectroscopy (ICP-OES, Agilent, Varian 700). Zeta potential was tested with Malvern potential tester (Zetasizer nano ZS90). Thermogravimetric analysis (TGA) was performed on Q600 (TA company) at a heating rate of 20 ^{o}C/min from room temperature to 800 ^{o}C. Brunauer-Emmett-Teller (BET) measurement was carried out to obtain the specific surface area. The pore size distribution (PSD) was calculated from the adsorption branches of the isotherms using the DFT model. Emulsion droplets were observed using a German Leica DM500P optical microscope. Ultraviolet-visible spectra (UV-vis) were recorded using an Agilent Cary 60 UV-visible spectrophotometer at room temperature.

3. Figures and Figure Captions

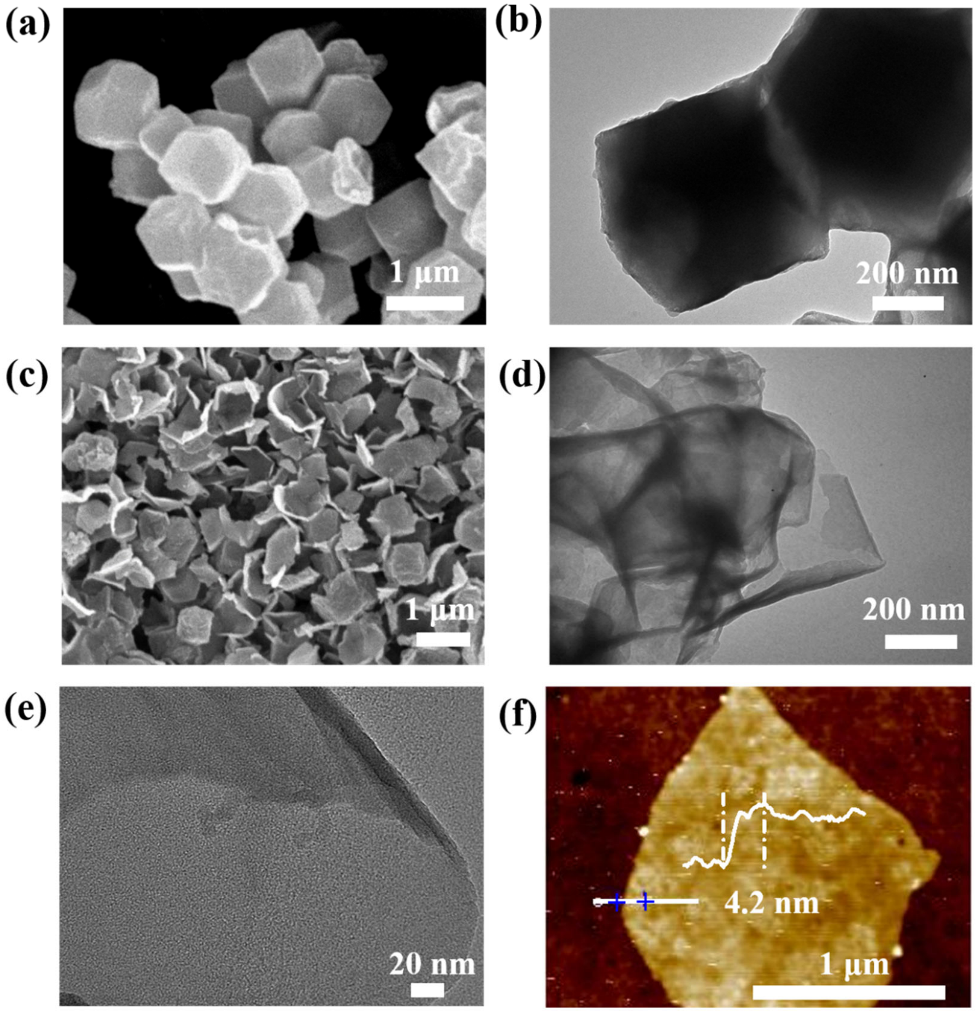

Figure S1. (a) SEM and (b) TEM images ZIF-67@(SiO_2/CTAB) core@shell nanoparticles (NPs). (c) SEM and (d) TEM images mSiO_2 nanosheets after etching away ZIF-67 core. (e) HRTEM image and (f) AFM height image of the mSiO_2 nanosheets after removal of ZIF-67 core.

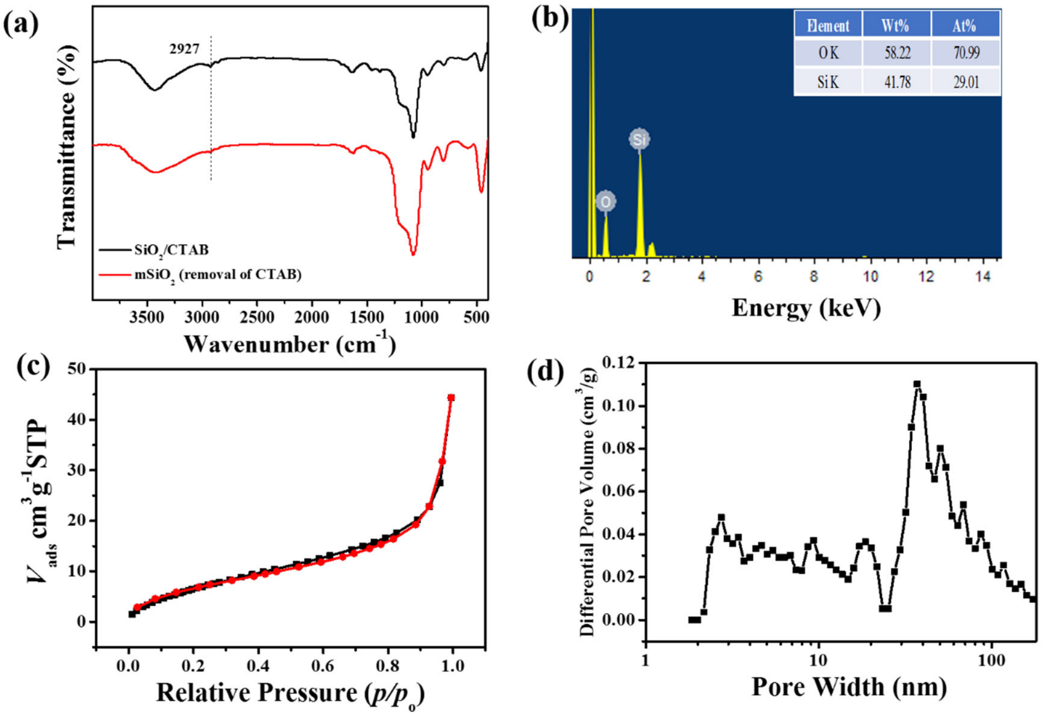

Element	Wt%	At%
O K	58.22	70.99
Si K	41.78	29.01

Figure S2. (a) FT-IR of SiO$_2$ nanosheets before and after the removal of CTAB. (b) EDS spectrum of SiO$_2$ nanosheets after removing CTAB. (c) N_2 adsorption-desorption isotherm and (d) pore size distribution of SiO$_2$ nanosheets after removing CTAB.

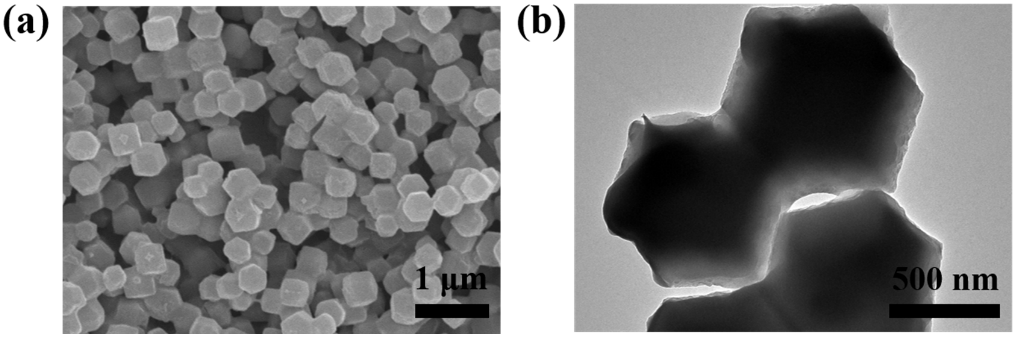

Figure S3. (c) SEM and (d) TEM images of ZIF-67@(SiO$_2$-NH$_2$/CTAB).

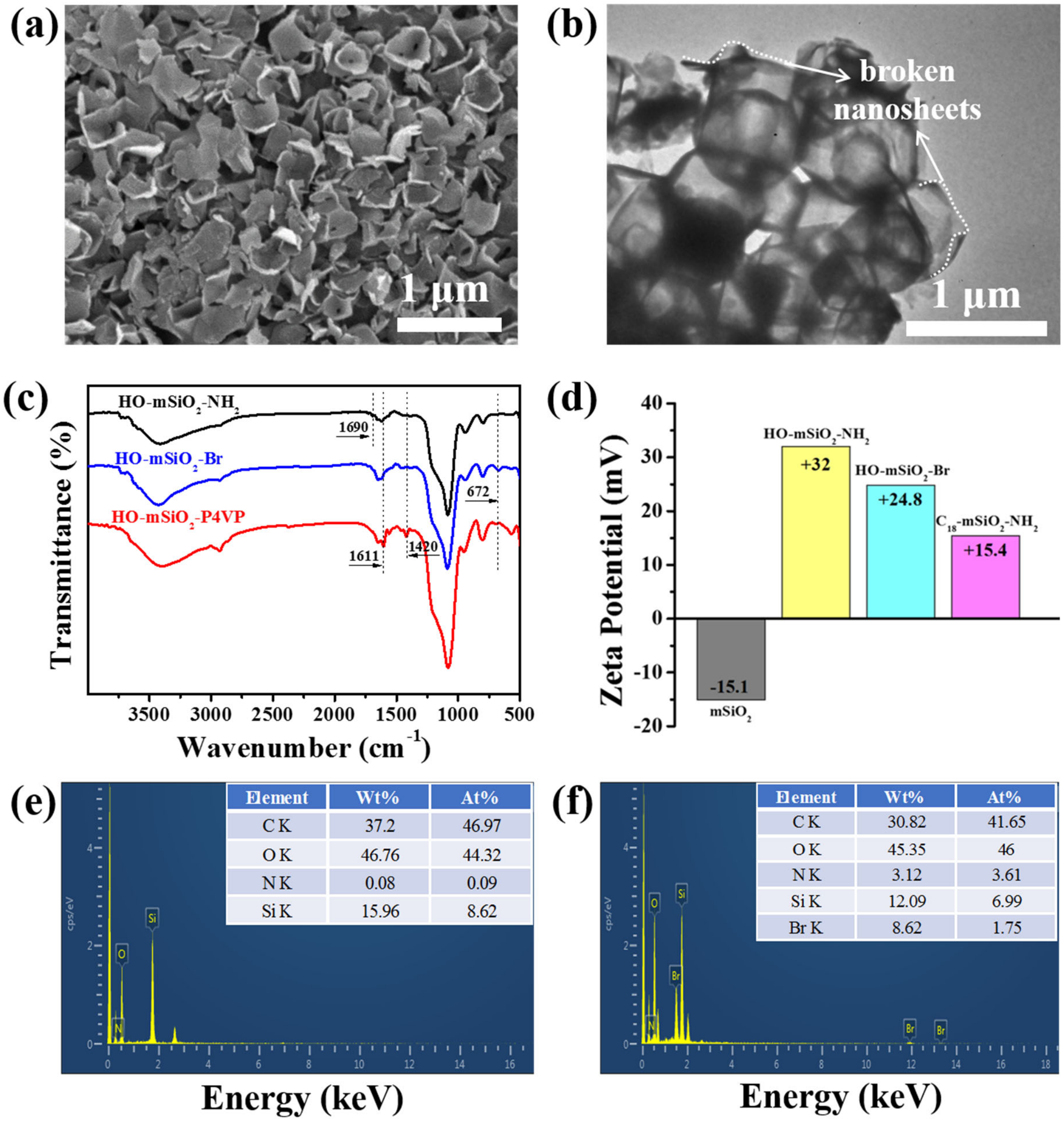

(e)

Element	Wt%	At%
C K	37.2	46.97
O K	46.76	44.32
N K	0.08	0.09
Si K	15.96	8.62

(f)

Element	Wt%	At%
C K	30.82	41.65
O K	45.35	46
N K	3.12	3.61
Si K	12.09	6.99
Br K	8.62	1.75

Figure S4. (a) SEM and (b) TEM images of HO-mSiO$_2$-NH$_2$ Janus mesoporous nanosheets (JMNs). (c) FT-IR spectra of HO-mSiO$_2$-NH$_2$, HO-mSiO$_2$-Br and HO-mSiO$_2$-P4VP. (d) Zeta potential of pristine mSiO$_2$ (i.e., HO-mSiO$_2$-OH with hydroxyl group (-OH) on the opposite side, control sample, see *Experimental Section*), HO-mSiO$_2$-NH$_2$, HO-mSiO$_2$-Br, and C$_{18}$-mSiO$_2$-NH$_2$. EDS spectra of (e) HO-mSiO$_2$-NH$_2$ and (f) HO-mSiO$_2$-Br.

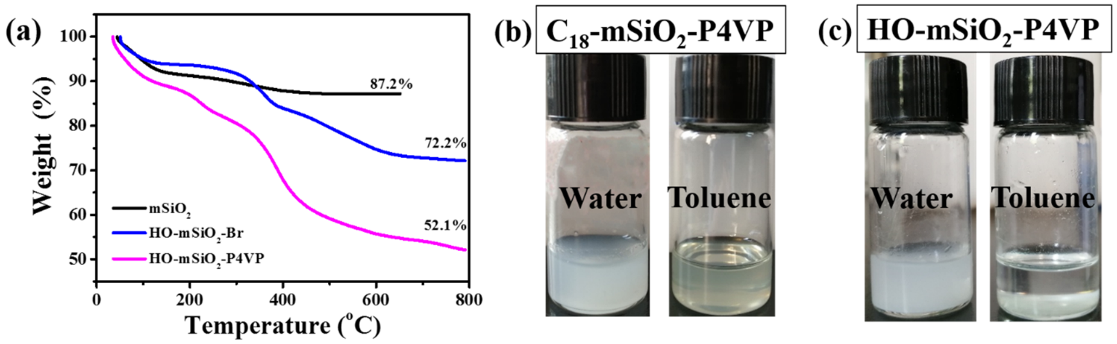

Figure S5. (a) Thermogravimetric analysis (TGA) curves of pristine mSiO$_2$ (control sample, see *Experimental Section*), HO-mSiO$_2$-Br and HO-mSiO$_2$-P4VP. Digital images of (b) C$_{18}$-mSiO$_2$-P4VP and (c) HO-mSiO$_2$-P4VP dispersed in water and toluene, respectively.

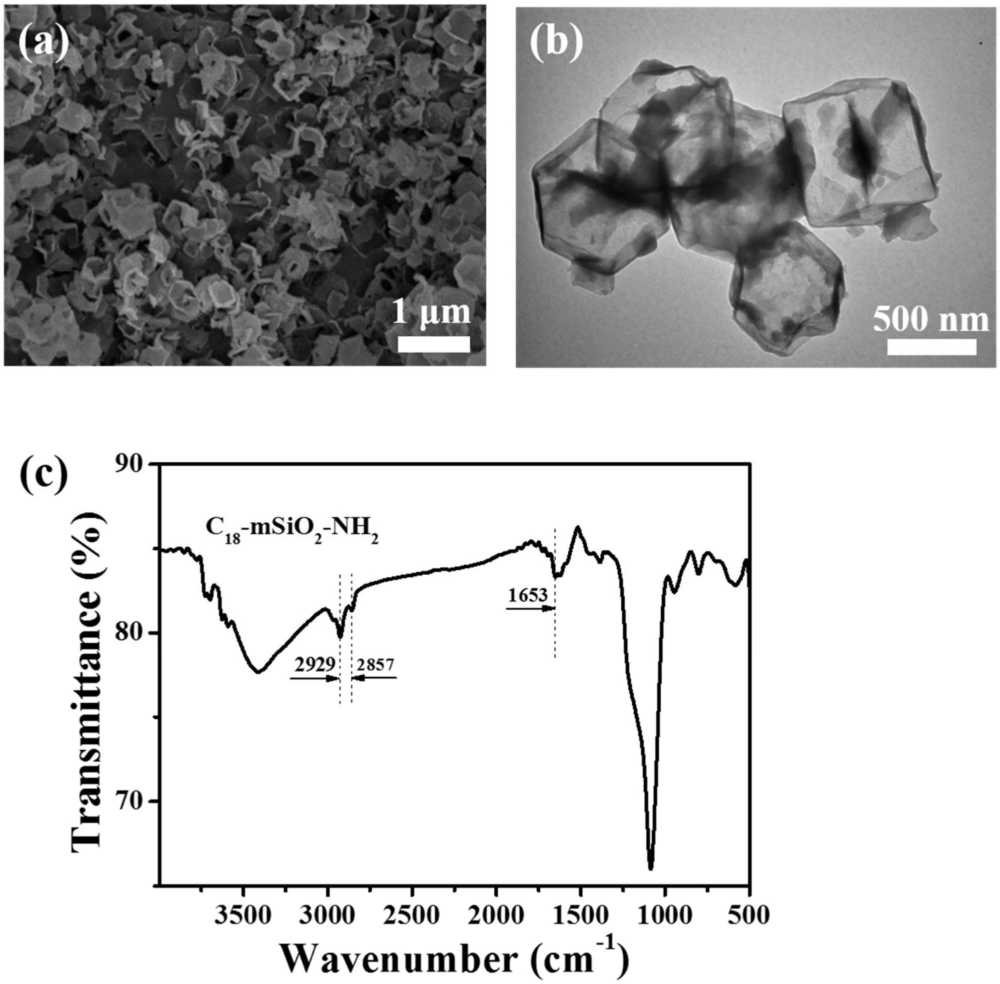

Figure S6. (a) SEM, (b) TEM and (c) FI-IR spectrum of C_{18}-$mSiO_2$-NH_2 JMNs.

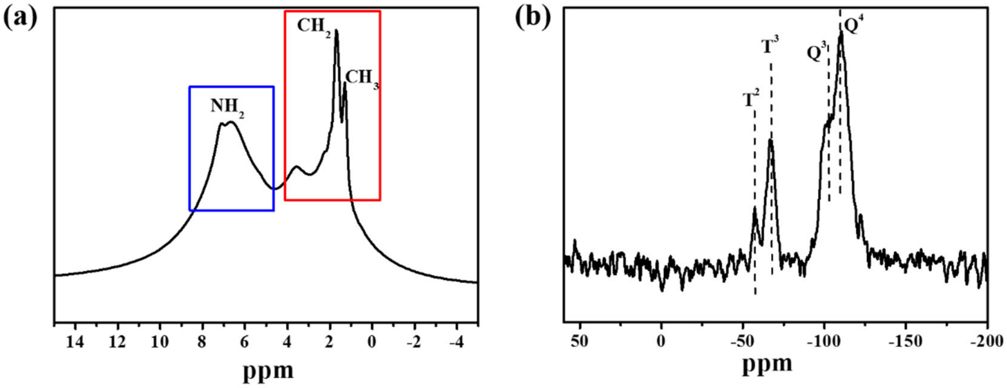

Figure S7. (a) ^1H MAS NMR and (b) ^{29}Si MAS NMR spectra of C_{18}-$mSiO_2$-NH_2 JMNs.

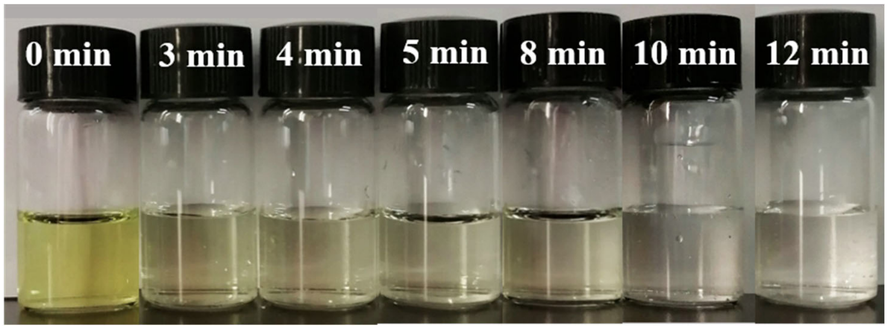

Figure S8. Digital images of the samples (i.e., a mixture of 4-NP and 4-AP) collected at different reaction times catalyzed by C_{18}-mSiO_2-P4VP@Au JMNs at pH = 6.

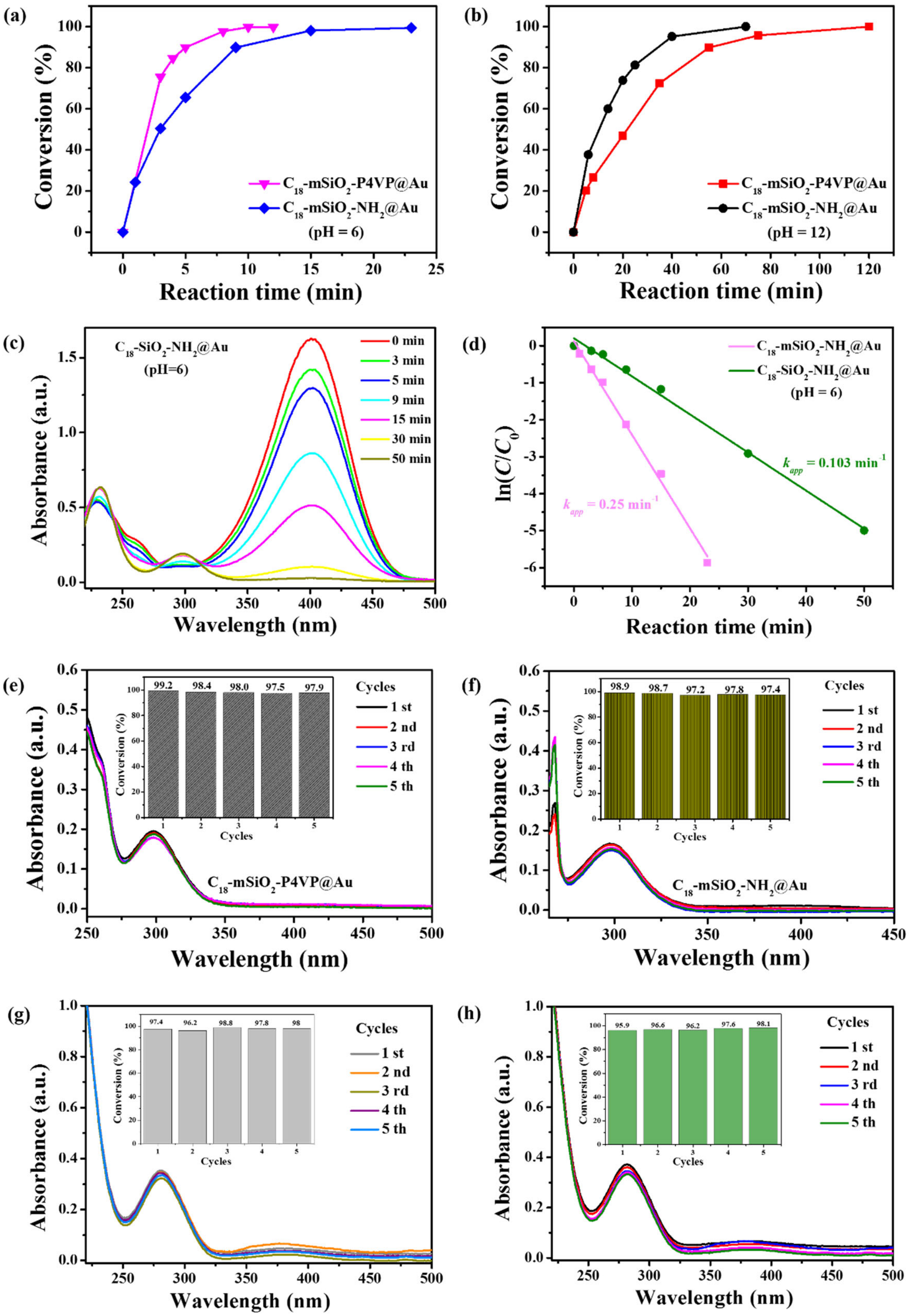

Figure S9. (a-b) The conversion of 4-nitrophenol (4-NP) to 4-aminophenol (4-AP) in aqueous solution as a function of reaction time, catalyzed by C_{18}-mSiO$_2$-P4VP@Au and C_{18}-mSiO$_2$-NH$_2$@Au JMNs at (a) pH = 6 and (b) pH = 12. (c) The UV spectra of the samples (i.e., a mixture of 4-NP and 4-AP) catalyzed by C_{18}-SiO_2-NH_2@Au JMNs under the same reaction conditions as C_{18}-mSiO_2-NH_2@Au JMNs. (d) ln C/C_0 of 4-NP as a function of reaction time at pH = 6 catalyzed by C_{18}-SiO_2-NH_2@Au JMNs and C_{18}-mSiO_2-NH_2@Au JMNs, respectively. UV-vis spectra of the samples collected after the catalytic reaction was completed, by exploiting the recycled (e) C_{18}-mSiO_2-P4VP@Au and (f) C_{18}-mSiO_2-NH_2@Au JMNs, respectively, as catalysts at pH = 6; by employing the recycled (g) C_{18}-mSiO_2-P4VP@Au and (h) C_{18}-mSiO_2-NH_2@Au JMNs, respectively, as catalysts at pH = 12. Insets are the histograms of the conversion. Recyclability of the as-prepared Janus-type catalysts was characterized by both UV-vis spectroscopy and conversion.

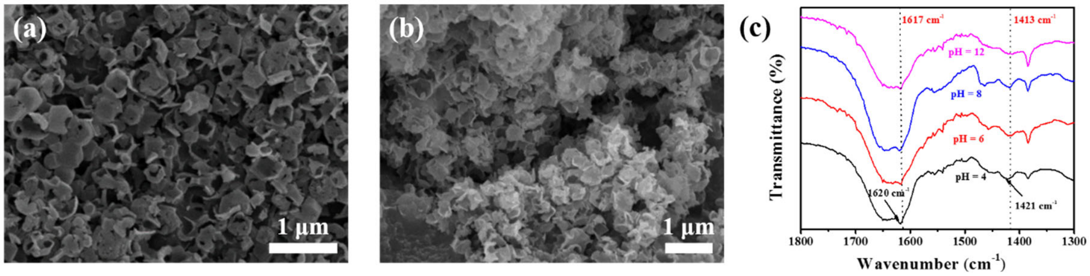

Figure S10. SEM images of C_{18}-mSiO_2-P4VP@Au JMNs dispersed in aqueous solution at (a) pH = 6 and (b) pH = 12. (c) FTIR spectra of C_{18}-mSiO_2-P4VP JMNs at various pH values.

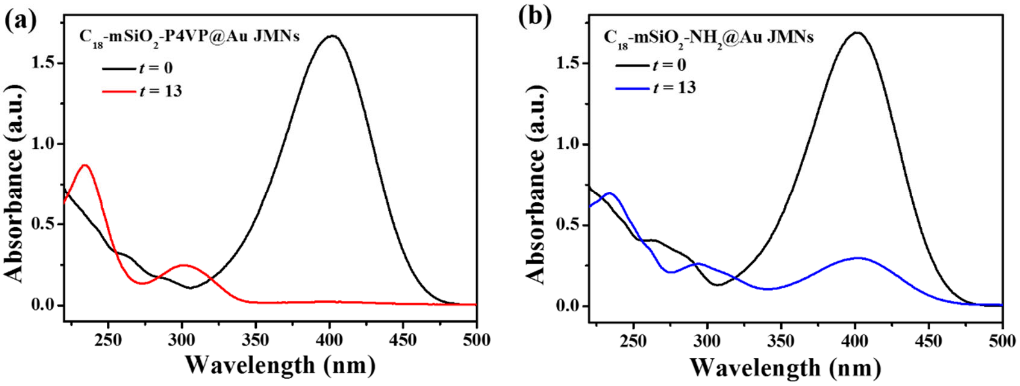

Figure S11. The recovered catalytic performance of C_{18}-mSiO_2-P4VP@Au JMNs and C_{18}-mSiO_2-NH_2@Au JMNs collected from the reaction systems at pH = 12 and redispersed into fresh 4-nitrophenol solution at pH = 6. The UV spectra demonstrated that 4-nitrophenol was almost converted into 4-aminophenol at *t* =13 min catalyzed by C_{18}-mSiO_2-P4VP@Au JMNs, and 85% was converted under the catalysis of C_{18}-mSiO_2-NH_2@Au JMNs, matching well with the results obtained from the fresh catalysts.

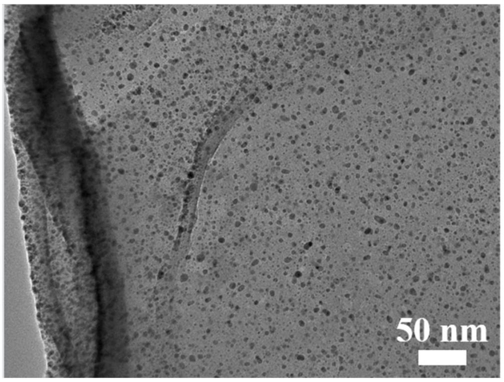

Figure S12. TEM images of C_{18}-mSiO_2-P4VP@Au JMNs after heating at 80 °C for 12 h.

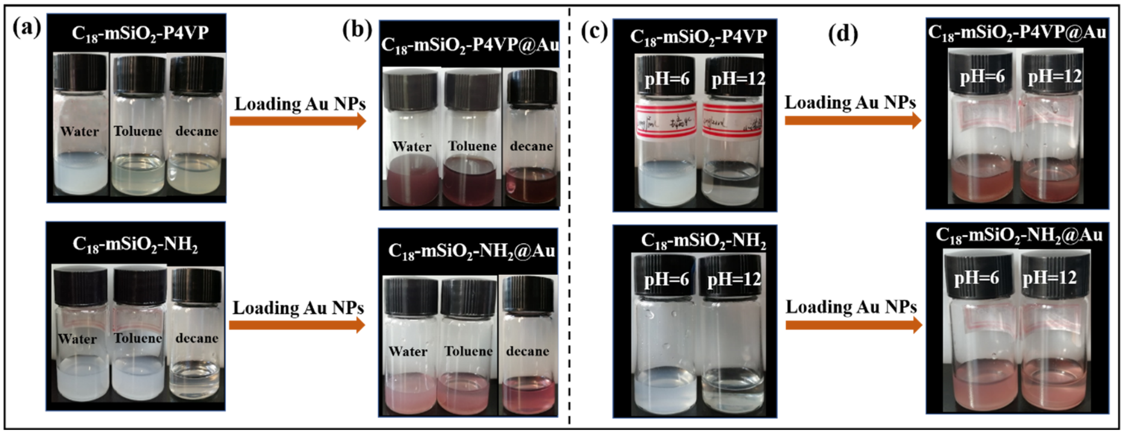

Figure S13. Photographs of the dispersions of (a) C_{18}-mSiO_2-P4VP (upper) and C_{18}-mSiO_2-NH_2 (lower) JMNs in water (pH = 6), toluene and decane, respectively; (b) C_{18}-mSiO_2-P4VP@Au (upper) and C_{18}-mSiO_2-NH_2@Au (lower) JMNs in water (pH = 6), toluene and decane, respectively; (c) C_{18}-mSiO_2-P4VP and C_{18}-mSiO_2-NH_2 JMNs in water at pH = 6 and pH = 12, respectively; and (d) C_{18}-mSiO_2-P4VP@Au (upper) and C_{18}-mSiO_2-NH_2@Au (lower) JMNs in water at pH = 6 and pH = 12, respectively.

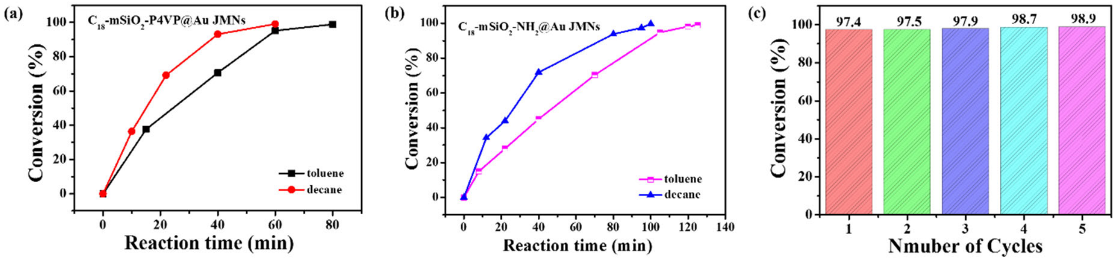

Figure S14. The conversion of 4-nitroanisole to 4-aminoanisole as a function of reaction time: (a) catalyzed by C_{18}-mSiO_2-P4VP@Au JMNs with toluene and decane as the oil phase, respectively, and (b) catalyzed by C_{18}-mSiO_2-NH_2@Au JMNs with toluene and decane as the oil phase, respectively. (c) A histogram of the conversion of 4-nitroanisole catalyzed by recycled C_{18}-mSiO_2-NH_2@Au JMNs with toluene as the oil phase.

4. Reference

(1) Hou, Y.; Wen, Z. H.; Cui, S. M.; Ci, S. Q.; Mao, S.; Chen, J. H. An Advanced Nitrogen-Doped Graphene/Cobalt-Embedded Porous Carbon Polyhedron Hybrid for Efficient Catalysis of Oxygen Reduction and Water Splitting. *Adv. Funct. Mater.* **2015**, *25*, 872-882.